RSC Advances

PAPER

Cite this: *RSC Adv.*, 2016, **6**, 38964

Hybrid mesoporous Cu_2ZnSnS_4 (CZTS)–TiO_2 photocatalyst for efficient photocatalytic conversion of CO_2 into CH_4 under solar irradiation†

Kidon Kim,[a] Abdul Razzaq,[a] Saurav Sorcar,[a] Yiseul Park,[b] Craig A. Grimes[a] and Su-Il In*[a]

Received 30th January 2016
Accepted 4th April 2016

DOI: 10.1039/c6ra02763f

www.rsc.org/advances

A major concern facing global society is the ongoing excessive release of CO_2 into the atmosphere where it acts as a heat-trapping greenhouse gas. One approach to helping control atmospheric CO_2 concentrations is to use solar energy to convert CO_2 into useful products, namely hydrocarbons, by use of specifically designed photocatalytic materials. While numerous photocatalysts have been investigated for use in CO_2 reduction, the field remains in it's infancy with, overall, relatively poor photoconversion efficiencies and product selectivity. This study reports the synthesis and design of a mesoporous noble metal free p-type Cu_2ZnSnS_4 (CZTS)/n-type TiO_2 heterojunction photocatalyst for broad spectrum light absorption, enhanced charge separation and transfer that, in turn, enhances photocatalytic CO_2 conversion. A maximum methane production rate of 118.75 ppm g^{-1} h^{-1} is observed, which represents a methane evolution rate approximately 12 times greater than that of pure TiO_2. The key factors contributing to the enhanced photocatalytic performance seen in the mesoporous CZTS–TiO_2 samples include improved light absorption, high surface area, and effective charge separation.

1. Introduction

The significant rise in atmospheric CO_2 concentration since the onset of the industrial revolution, due primarily to the combustion of hydrocarbon fuels, has generated considerable, and in the opinion of the authors justified, concern.[1] An effective approach to mitigate this problem would be to use solar energy to convert CO_2 into hydrocarbon fuels compatible with the current energy infrastructure through photocatalysis.[2] The concept is an appealing one, offering a ready means for storing and transporting solar energy; further, such fuels could be obtained on a sustainable, rather than one-shot, basis. To emphasize the underlying opportunity: the use of sunlight to efficiently convert CO_2 and H_2O into hydrocarbon fuels offers the dual advantages of minimizing the potential for severe global climatic disruptions while obtaining low-cost renewable fuels.[3]

Among photocatalysts, anatase TiO_2-based materials offer advantages that include relatively low cost, excellent photocorrosion stability and photo-oxidation power, non-toxicity, and rapid transfer of photon-generated charges.[4–7] A prodigious amount of work has been done to try and lower the bandgap of TiO_2 in an attempt to better utilize solar energy. Such efforts include, for example, loading the TiO_2 with metal[8,9] or non-metal elements,[10–15] and so on, all of which have been largely unsuccessful: that which lowers the bandgap lowers the mobility of the generated charges. However such efforts continue, and in the opinion of the authors serve as a worthy objective. For example, Zhu and co-workers have reported S-doped TiO_2 possessing highly efficient photocatalytic performance under indoor sunlight irradiation for degradation of organic pollutants; the catalyst was reported to be highly stable even after several months of indoor sunlight illumination.[16] The same authors have also reported a binary composite system harnessing the properties of two dimensional (2D) ultrathin carbon nitride (C_3N_4) nanosheets and NiS nanoparticles, with high hydrogen generation efficiency.[17] Graphene based materials have been investigated, such as ultra-thin conductive reduced graphene oxide sheets coupled with Ag[18] and rGO–TiO_2 nanotubes[19] aimed towards, respectively, photocatalytic oxidation of pollutants and CO_2 photoreduction.

Loading of noble metals within or on TiO_2 based materials as a co-catalyst is an effective but expensive way of improving electron–hole separation. We believe a sound approach to achieve a high performance photocatalyst in a cost effective

[a]*Department of Energy Systems Engineering, DGIST, 50-1, Sang-ri, Hyeonpung-myeon, Dalseoung-gun, Daegu-711-873, Republic of Korea. E-mail: insuil@dgist.ac.kr; Fax: +82-53-785-6409; Tel: +82-53-785-6417*

[b]*Division of Nano and Energy Convergence Research, DGIST, Republic of Korea*

† Electronic supplementary information (ESI) available: Schematic of experimental setup for photocatalytic CO_2 conversion test; TEM images of all hybrid CZTS–TiO_2 samples; FE-SEM EDS of CT4 sample; UV-vis DRS of as synthesized TiO_2 (air and Ar annealed); high resolution XPS of as-synthesized TiO_2 nanoparticles, and as-synthesized CZTS nanoparticles; BET surface areas for all hybrid CZTS–TiO_2 samples; stability tests of CT4 sample; turnover numbers and turnover frequencies for all hybrid CZTS–TiO_2 samples. See DOI: 10.1039/c6ra02763f

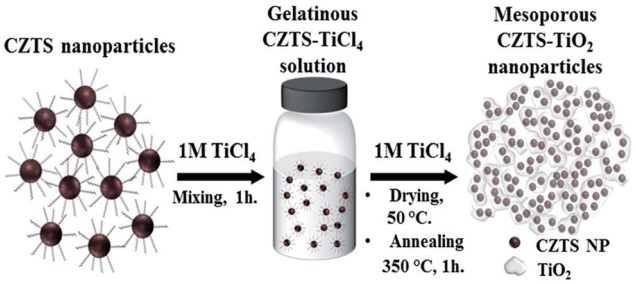

Fig. 1 Schematic showing the experimental strategy for synthesis of hybrid mesoporous CZTS–TiO_2 photocatalyst.

manner is to combine n-type TiO_2 with a non-toxic, earth-abundant and hence inexpensive p-type semiconductor that serves as a strong light-absorber. To that end, Cu_2ZnSnS_4, or CZTS, a p-type semiconductor with a direct bandgap of 1.5 eV, has recently emerged as an excellent photovoltaic material platform,[20–22] however its use as a photocatalyst for light-to-chemical energy conversion remains unexplored. Motivated by the unique qualities of CZTS and the opportunity for achieving improved photocatalytic properties by realization of a p–n junction type heterostructured material we have investigated, and herein report on a hybrid mesoporous CZTS–TiO_2 photocatalyst. The material manifests significant CO_2 reduction properties that can be attributed to broad-spectrum light absorption, the high surface-area mesoporous structure, and the intrinsic p–n junction nature of the mesoporous material for improved charge separation. Notably, we synthesize the mesoporous CZTS–TiO_2 without the use of any noble metal co-catalysts, yet still find significant CO_2 reduction at ambient temperature and pressure.

Our CZTS–TiO_2 synthesis strategy shown in Fig. 1 uses a simple, low-cost two-step process: CZTS nanoparticles are prepared by hot injection; the resulting CZTS nanoparticles are dispersed in toluene under an argon atmosphere, then vigorously mixed with $TiCl_4$ in toluene resulting in a gelatinous solution, subsequently annealed within an argon atmosphere resulting in the desired photocatalyst. A series of hybrid CZTS–TiO_2 samples were synthesized with varied amounts of CZTS in $TiCl_4$ (TiO_2 precursor). The obtained materials are labelled as CT1, CT2, CT3 and CT4 for the samples obtained with 1.9 mg, 3.8 mg, 5.7 mg and 7.6 mg of CZTS nanoparticles in 0.1 mL of $TiCl_4$ respectively. We believe our work will help lead to more cost-effective, high-performance photocatalysts for the conversion of solar energy to chemical fuels.

2. Experimental section

2.1. Materials

Copper(II) acetylacetonate (99.99%), zinc acetate (99.99%), tin(IV) acetate (99%), oleylamine (OLA, 70%), trioctylphosphine oxide (TOPO, 99%) and titanium(IV) chloride (99.99%), and all chemicals, were purchased from Sigma Aldrich and used without further purification.

2.2. Synthesis of Cu_2ZnSnS_4 (CZTS) nanocrystals

CZTS nanocrystals were synthesized by the hot-injection method.[23] All reaction conditions were kept under inert atmosphere to prevent the formation of oxides. In a typical synthesis, a mixture of 0.5 mmol $Cu(acac)_2$, 0.25 mmol $Zn(OAc)_2$, 0.25 mmol $Sn(OAc)_4$, and 4.0 mL OLA was prepared in a 25.0 mL 3-neck round-bottom reaction flask and heated under vacuum to 150 °C for 30 minutes. A change in the color of the metals solution was observed from blue to brown-green. The temperature was lowered to 125 °C and the mixture remained at this temperature under vacuum until injection. In a 5.0 mL scintillating vial, 1.0 mM sulfur powder was sonicated for 30 minutes with 1.0 mL OLA to achieve its complete dissolution resulting in an orange-red solution. In a 50.0 mL 3-neck round–bottom reaction flask, 10 mM TOPO was heated to 300 °C on an argon Schlenk line. When the temperature of the TOPO reaction flask reached 100 °C, the flask was pumped and purged three times in order to remove any adsorbed water vapors and impurities, then flushed with Ar and kept under argon for the remainder of the experiment. When the TOPO reaction temperature reached 300 °C, the S and metal precursors were rapidly injected simultaneously *via* two gas-tight Luer-Lock syringes. The reaction solution immediately changed from clear and colorless to a clear dark brown solution. All the aliquots were taken out using a syringe. 18.0 mL methanol was added to the aliquots to precipitate the nanocrystals, followed by 10 minutes of centrifugation at 3500 rpm. The supernatant, containing unreacted material was discarded, while the remaining precipitate was then redispersed in 8.0 mL toluene to which 10.0 mL methanol was again added and the solution centrifuged for 10 minutes. This process was repeated for a total of three washes. The final precipitate was re-suspended in toluene and then centrifuged for 10 minutes to remove any agglomerated or bulk constituents.

2.3. Synthesis of hybrid mesoporous Cu_2ZnSnS_4 (CZTS)–TiO_2 photocatalyst

As synthesized CZTS nanocrystals were oven dried at 80 °C overnight to remove toluene and obtain a powder of CZTS nanocrystals. CZTS–TiO_2 samples were prepared by mixing various amounts of CZTS powder in fixed volume *i.e.* 0.1 mL of $TiCl_4$ under argon atmosphere for 1 h. The samples were named as CT1, CT2, CT3 and CT4 standing for 1.9 mg, 3.8 mg, 5.7 mg and 7.6 mg of CZTS in 0.1 mL of $TiCl_4$ respectively. The various obtained samples were dried at 50 °C in order to remove toluene and then were annealed at 350 °C (rate time: 5°C min^{-1}, holding time 1 h under argon gas flow of 30 cm^3 min^{-1}).

2.4. Photocatalyst characterizations

The crystalline structure of the materials are analyzed by powder X-ray diffractometry (XRD, Panalytical, Empyrean; operating at 40 kV and 30 mA with Cu Kα radiation, $\lambda = 1.54$ Å, as an X-ray source, scanned with a rate of 1° min^{-1} in the range of $2\theta = 10°$–$70°$). High resolution images are obtained using field emission transmission electron microscopy (FE-TEM,

Hitachi HF-3300) operating at 300 kV. For FE-TEM analysis, the samples are prepared by dispersing in ethanol followed by mild sonication. The dilute suspension is dropped on a TEM Cu mesh grid and allowed to dry overnight. The elemental composition of sample CT4 is measured using the energy dispersive spectroscopy (EDS) attachment of the Hitachi S-4800 FE-SEM; the electron energy was 15 keV for the EDS measurement. UV-visible diffuse reflectance spectroscopy (DRS) of the materials is measured using a Cary series UV-visible near IR spectrophotometer with a diffuse reflection accessory. The N_2 sorption isotherms are measured at −196 °C on a Micromeritics ASAP 2000 apparatus, with the samples extensively degassed at 200 °C prior to the experiments. Surface areas are calculated by the Brunauer–Emmett–Teller (BET) equation. The pore volume is determined from the amount of N_2 adsorbed at the highest relative pressure of $(P/P_0) = 0.99$. The BJH pore diameter is obtained by applying the Barrett–Joyner–Halenda (BJH) equation to the desorption isotherm. The surface composition and oxidation states are determined by X-ray photoelectron spectroscopy (XPS, Thermo VG, K-alpha) using the Al Kα line (148 606 eV) as the X-ray source.

2.5. Photocatalytic CO_2 conversion test method

Photocatalytic CO_2 conversion experiments are performed in a gas phase reactor as reported earlier.[24] In short, the photoreactor (stainless steel with quartz window, volume = 15.4 cm^3) is loaded with a photocatalyst material (50 mg) and then purged with CO_2 gas (1000 ppm in He) and vacuum simultaneously to remove any air or other impurities. CO_2 gas (1000 ppm in He) is passed through a water bubbler, forming a mixture of CO_2 and H_2O vapors which then enters the photoreactor. The photoreactor is exposed to simulated solar light irradiated by Xenon solar simulator (Oriel, LCS-100) with an AM 1.5 filter for variable durations and the reaction products (500 μL) analyzed by a Shimadzu GC-2014 gas chromatograph (Restek Rt-Q Bond column, ID = 0.53 mm, length = 30 m) equipped with flame ionization detector (FID) and thermal conductivity detector (TCD). A schematic showing the experimental setup for photocatalytic CO_2 reduction is shown in Fig. S1.† The hour-normalized photocatalytic CH_4 evolution rate is calculated by:

$$\text{Rate of } CH_4 \text{ evolution} = \frac{\text{amount of } CH_4 \text{ evolved (ppm)}}{\text{amount of photocatalyst used (g)}}$$

To examine photocatalyst stability, under otherwise identical experimental conditions sample CT4 was illuminated for 5 h and 10 h durations.

3. Results and discussion

3.1. Characterization of hybrid mesoporous CZTS–TiO_2 photocatalyst

Fig. 2 shows a transmission electron microscopy (TEM) image of as-synthesized CZTS nanoparticles; one sees anisotropic shapes with an average size of 13 nm. High resolution transmission electron microscopy (HRTEM) indicates an interplanar spacing of 3.1 Å corresponding to d_{112} of CZTS (Fig. 2b).[20] The selected area electron diffraction (SAED) pattern supports the polycrystalline nature of CZTS by displaying rings indexed to d_{112}, d_{220} and d_{312} of CZTS, respectively (Fig. 2c).[25] The TEM image of representative hybrid CZTS–TiO_2, sample CT4, synthesized from 7.6 mg CZTS in 0.1 mL $TiCl_4$, clearly demonstrate the post-annealing mesoporous nature (Fig. 2d). The obtained mesoporosity of the hybrid system can be attributed to the removal of the capping ligands during annealing, imparting both the mesoporous nature and hybridization of TiO_2 with CZTS. Fig. 2e is a HRTEM image of a hybrid CZTS–TiO_2 sample, showing a lattice spacing of 3.1 Å and 3.5 Å, corresponding to d_{112} plane of CZTS and d_{101} plane of TiO_2 respectively.[20,26] The selected area electron diffraction (SAED) pattern show rings which can be indexed to d_{112} plane of CZTS,[20] and d_{101} plane of anatase TiO_2 (ref. 25 and 27) further assuring the formation of hybrid CZTS–TiO_2 structure (Fig. 2f). The mesoporous nature of all annealed CZTS–TiO_2 samples is confirmed by TEM (Fig. S2†).

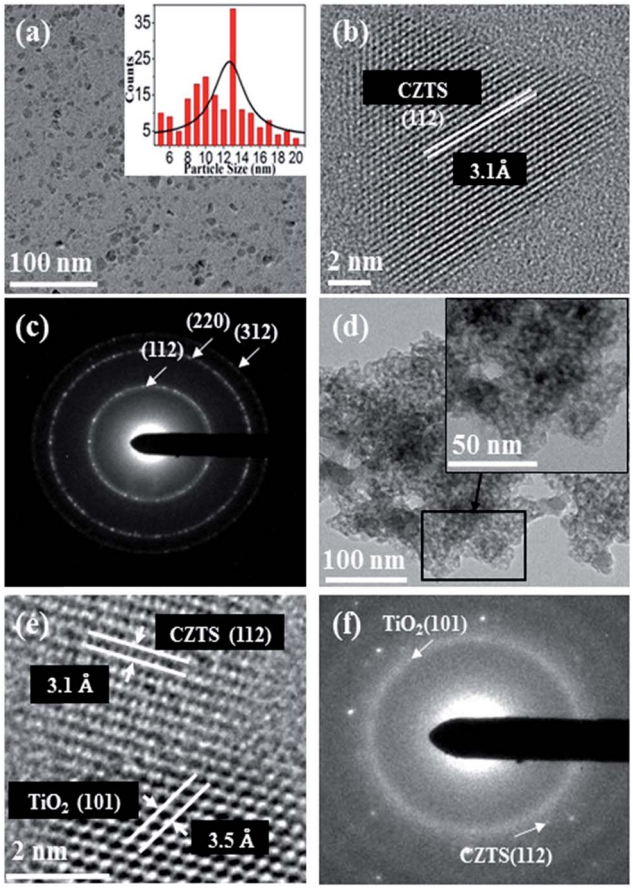

Fig. 2 TEM, HRTEM and SAED patterns of: (a–c) as synthesized CZTS nanoparticles; and (d–f) CZTS–TiO_2 sample CT4.

Fig. 3 shows the elemental analysis of sample CT4 using energy dispersive X-ray scanning transmission electron microscopy (EDX-STEM); the representative sample consists of Ti, O, Cu, Zn, Sn and S, confirming the formation of a hybrid CZTS–TiO_2 photocatalyst. Further, the uniform color suggests the uniform distribution of elements.

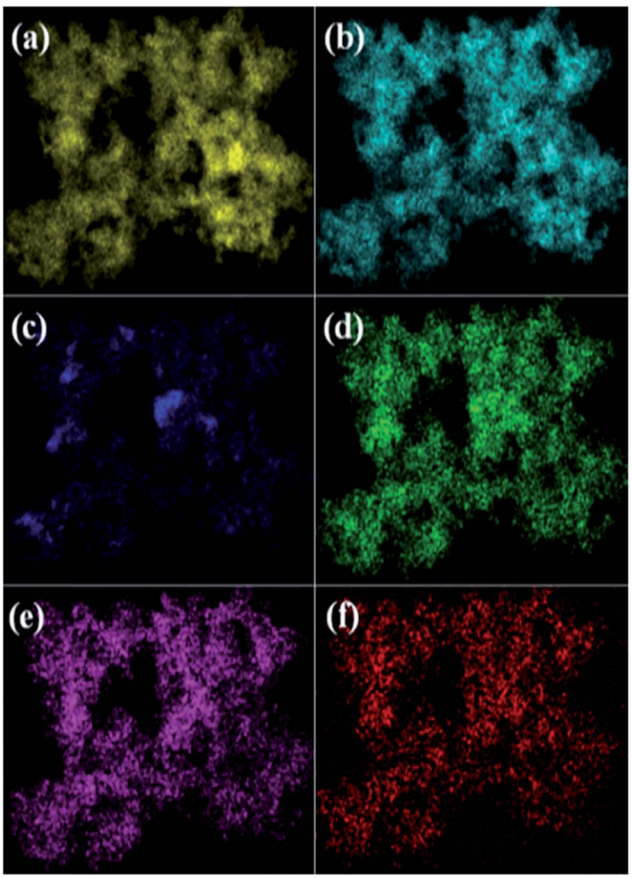

Fig. 3 EDX-STEM elemental mapping image of CT4 sample showing composition of: (a) titanium, (b) oxygen, (c) copper, (d) zinc, (e) tin, and (f) sulphur.

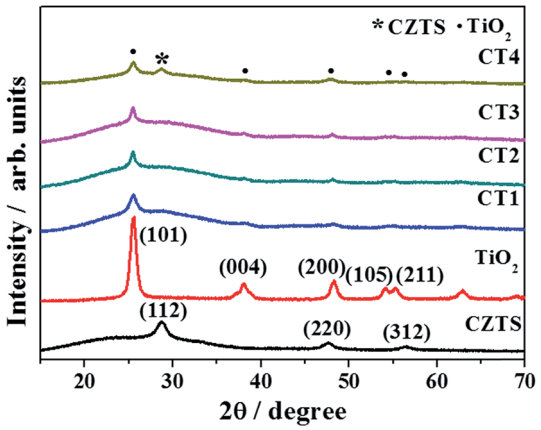

Fig. 4 XRD pattern for as-synthesized CZTS, TiO_2 and hybrid CZTS–TiO_2 samples (CT1, CT2, CT3 and CT4 stands for 1.9, 3.8, 5.7 and 7.6 mg of CZTS in 0.1 mL of $TiCl_4$ respectively).

The atomic composition of sample CT4, obtained using FESEM-EDS, is shown in Fig. S3; † the rectangular region scan shows strong peaks associated with Cu, Zn, Sn, S, Ti and O. However, the atomic ratios of Sn and S in CZTS are less than anticipated, which we suggest can be attributed to diffusion of SnS/S_2 gases due to *in situ* annealing while being FESEM-EDS imaged,[28] or while sample-annealing under argon atmosphere for CT4 synthesis. We are not the only investigators to encounter this; a loss of Sn and S is reported to be one of the critical problems encountered during CZTS synthesis.[29,30]

X-ray diffraction (XRD) of as-synthesized TiO_2, CZTS, and hybrid CZTS–TiO_2 photocatalysts are shown in Fig. 4. CZTS nanoparticles indicate peaks at 2θ values of 28.53°, 47.33°, and 56.17° corresponding to d_{112}, d_{220} and d_{312} of Kesterite CZTS.[31] The XRD pattern of the TiO_2 sample prepared from $TiCl_4$ clearly shows peaks at 2θ values of 25.28°, 37.80°, 48.05°, 53.89° and 55.06° corresponding to d_{101}, d_{004}, d_{200}, d_{105} and d_{211} of anatase TiO_2.[26] All CZTS–TiO_2 samples show peaks corresponding to anatase TiO_2, however the CZTS peaks are diffuse and appear as a relatively broad hump at $2\theta = 28.53°$, a behavior that might be attributed to the small size of CZTS nanoparticles. Upon increasing the CZTS amount within the hybrid CZTS–TiO_2 samples, CT4 synthesized from 7.6 mg CZTS in 0.1 mL $TiCl_4$, the XRD peak for Kesterite CZTS at $2\theta = 28.53°$ becomes more prominent, confirming the CZTS presence.

The UV-vis diffuse reflectance spectra (DRS) of bare TiO_2 annealed under air and argon atmosphere is shown in Fig. S4† and it exhibits a steep absorption edge in the range of 380–420 nm, corresponding to the fundamental bandgap of 3.2 eV.[27] That the as-prepared TiO_2 nanoparticles absorb in the visible region can be attributed to the Urbach band tail, arising from the momentary localization of excitons due to phonon interaction.[34,35]

Fig. 5a shows the absorption spectrum of pure CZTS nanoparticles, showing broad absorption in the visible light range. The bandgap of the CZTS nanoparticles is estimated using the Tauc relationship, resulting in a band gap of 1.5 eV, a value consistent with reported literature values (1.45–1.6 eV).[23] In case of hybrid CZTS–TiO_2, a prominent enhancement in light absorption is observed in the visible light range (400–700 nm) with the increase in CZTS (Fig. 5b); the degree of CZTS content strongly affects the visible light absorption of TiO_2 leading to a red shift in the absorption spectrum.

Further evidence indicating a hybrid CZTS–TiO_2 material comes from X-ray photoelectron spectroscopy (XPS) data of sample CT4 (Fig. 6). The Ti 2p region shows two main peaks located at 463.9 eV and 458.3 eV corresponding to the Ti $2p_{1/2}$ and Ti $2p_{3/2}$ states respectively (Fig. 6a), while the O 1s region exhibits peak around 530.9 eV attributed to Ti(IV) ion bound oxygen, in TiO_2 (Fig. 6b).[32] Cu 2p region with the main characteristic peaks located at 931.2 eV and 951 eV, attributed to Cu $2p_{1/2}$ and Cu $2p_{3/2}$ electronic states respectively with the peak separation of 19.8 eV, assuring the presence of Cu(I) (Fig. 6c).[33] The XPS spectrum of Zn 2p splitting into two peaks appearing at 1020.9 eV and 1043.9 eV, can be assigned to Zn $2p_{1/2}$ and Zn $2p_{3/2}$ respectively (Fig. 6d). These two peaks display a peak separation of 23 eV, indicating presence of Zn(II).[34] The XPS spectrum of Sn 3d with the peaks at 486.1 eV and 494.5 eV are attributed to Sn $3d_{3/2}$ and Sn $2d_{5/2}$ of Sn(IV), Fig. 6e.[36] The S 2p region exhibits two main peaks appearing at 162.38 eV and 163.53 eV (Fig. 6f); these peaks can be assigned to S $2p_{1/2}$ and S

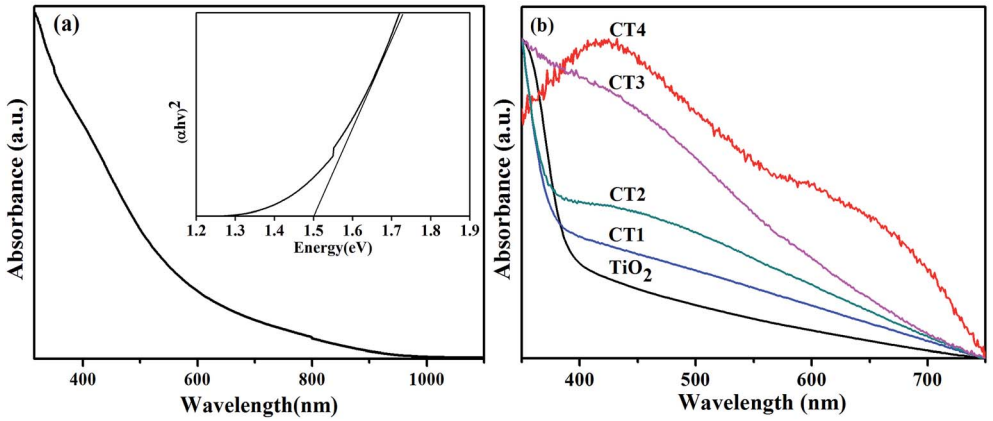

Fig. 5 UV-vis DRS spectra for: (a) as-synthesized CZTS nanoparticles, with the inset showing the determined band gap value of 1.5 eV; (b) CZTS–TiO_2 samples CT1, CT2, CT3 and CT4, which stand for, respectively, 1.9, 3.8, 5.7 and 7.6 mg of CZTS in 0.1 mL of $TiCl_4$.

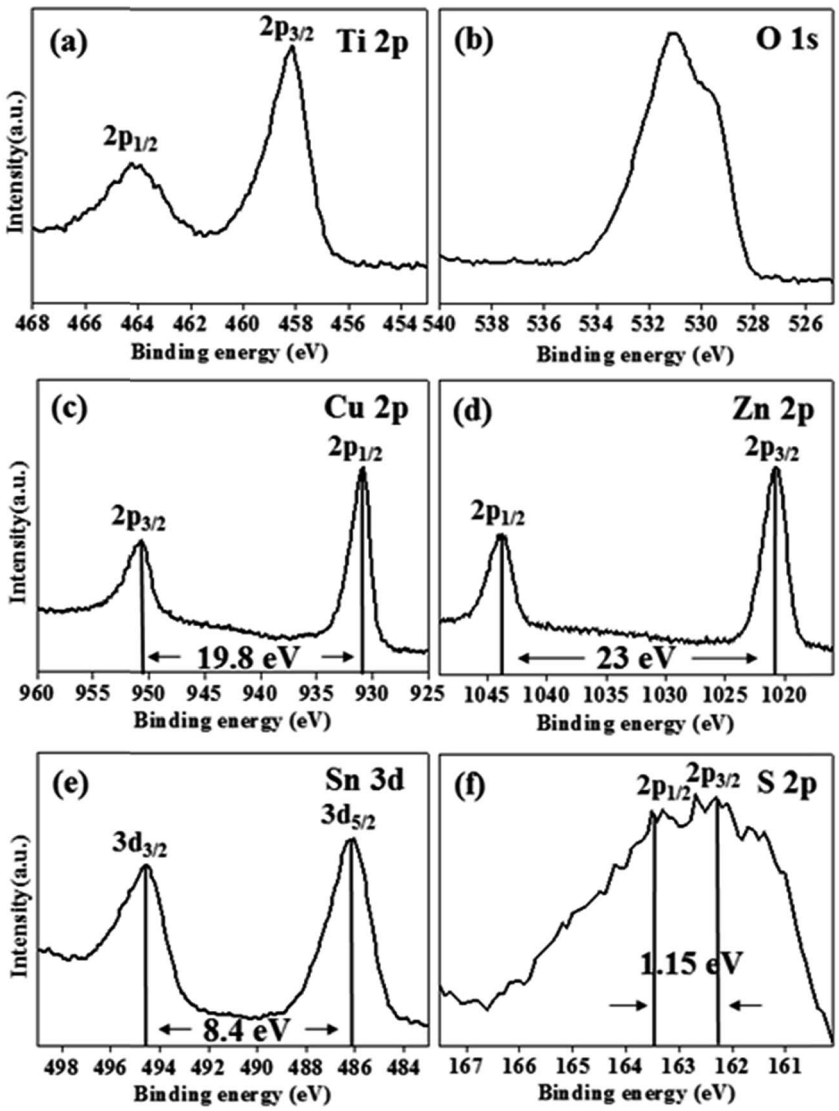

Fig. 6 X-ray photoelectron spectroscopy (XPS) of CT4 sample with regions of: (a) titanium, (b) oxygen, (c) copper, (d) zinc, (e) tin and (f) sulphur.

$2p_{3/2}$ with a peak separation of 1.15 eV confirming the presence of S.[37] XPS spectra for the as-prepared TiO_2 nanoparticles and pure CZTS nanoparticles were investigated to confirm the presence of all the respective elements in their expected oxidation states (Fig S5 and S6†); it is observed that all the corresponding peaks appearing for sample CT4, our representative sample, are in good agreement with the peaks of as-synthesized CZTS and TiO_2, thus assuring no significant change in the electronic states of the respective materials.

The Brunauer–Emmett–Teller (BET) surface areas are also measured for all hybrid CZTS–TiO_2 samples (Fig. S7 & Table S1†). The N_2-sorption isotherms of all samples, shown in Fig. S5,† are found to be of type IV according to IUPAC classification.[38] The samples initially exhibit a monolayer adsorption, which is followed by a steep rise indicating the multilayer adsorption phenomenon. The multilayer adsorption is then followed by condensation within the mesoporous material at high relative pressures. Due to difference in pressure of capillary evaporation and condensation, the isotherm exhibits H3 hysteresis loops revealing the presence of plate like particles with slit-like pores.[38] Among all samples, sample CT4 shows the highest surface area of 92.71 $m^2\ g^{-1}$. Further, the surface area of the hybrid CZTS–TiO_2 samples increase with the addition of CZTS nanoparticles, indicating the CZTS nanoparticles are largely responsible for inducing the mesoporous nature of the hybrid samples.

3.2. Photocatalytic CO_2 reduction

Photocatalytic activities of all hybrid CZTS–TiO_2 samples, TiO_2, and CZTS samples are investigated by examining their ability to drive the photocatalytic conversion of CO_2 and water vapor into hydrocarbon fuels, under simulated AM1.5G solar light, with TiO_2 (synthesized from $TiCl_4$ precursor) and pure CZTS nanoparticles used as baseline reference samples (Fig. 7). Gas chromatography (GC) analysis of the products showed predominantly methane as a main hydrocarbon product. The rate of methane production from each sample is obtained after 1 h of solar illumination.

It is obvious that all hybrid mesoporous CZTS–TiO_2 samples show an increase in CH_4 yield. On increasing the amount of CZTS in the hybrid samples CZTS–TiO_2 the CH_4 evolution increases, with highest value of methane evolution found for sample CT4 (118.75 ppm $g^{-1}\ h^{-1}$), respectively 11.97 times and 9.7 times higher than TiO_2 (9.92 ppm $g^{-1}\ h^{-1}$) and CZTS (12.29 ppm $g^{-1}\ h^{-1}$).

Illumination of sample CT4 in an Ar/H_2O (g) atmosphere under similar conditions served as a control test, in which one can see a negligible amount of CH_4, suggesting any organic impurities adsorbed on the surface of hybrid CZTS–TiO_2 composites having negligible involvement in the photocatalytic CH_4 evolution. Turnover numbers (TON) and turnover frequencies (TOF) for the hybrid CZTS–TiO_2 photocatalysts are obtained and presented in Table S2.† Amongst hybrid photocatalyts, for 1 h illumination sample CT4 yielded a TON of 1.48 and TOF of 1.48 h^{-1}. Under extended illumination it is observed that the TON slightly increases after 5 h, reaching a value of 1.67, then decreases to 0.90 for 10 h of continuous illumination.

It can be inferred from the control experiments that the CH_4 evolved during our normal experiments is mainly due to photoreduction of CO_2 and not a product of organic oxidation or surface bound organic species. The improved photocatalytic performance of our hybrid CZTS–TiO_2 samples can be inferred to: (1) improve light absorption; (2) enhance the surface area; and (3) improved charge separation *via* electric-field induced drift per formation of a p–n junction at the interface of p-type CZTS and n-type TiO_2.

Based upon these factors, an illustration of energy levels and suggested process for conversion of CO_2 and water vapor into methane is shown in Fig. 8. As revealed by XPS, hybrid samples contain both CZTS and TiO_2; the conduction band edge of CZTS is higher than the TiO_2 conduction band edge, while the TiO_2 valence band edge is more positive than the valence band edge of CZTS and the O_2/H_2O redox potential.[39] Upon illumination, the photo-generated electrons in CZTS can easily flow to the conduction band of TiO_2, and can reduce the adsorbed CO_2 whereas the holes migrate in the opposite direction to oxidize

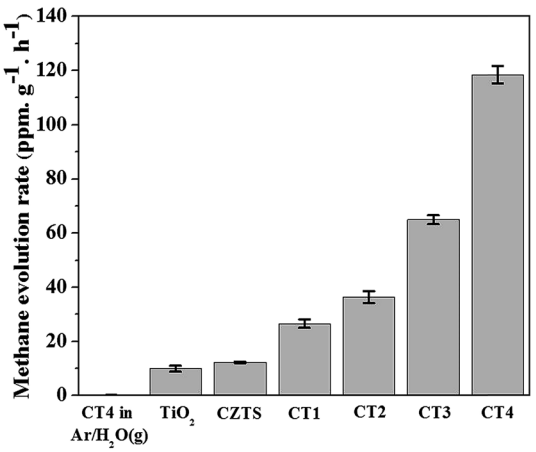

Fig. 7 Methane production rate for 1 h illumination from pure CZTS, TiO_2 and hybrid CZTS–TiO_2 samples under AM1.5G illumination.

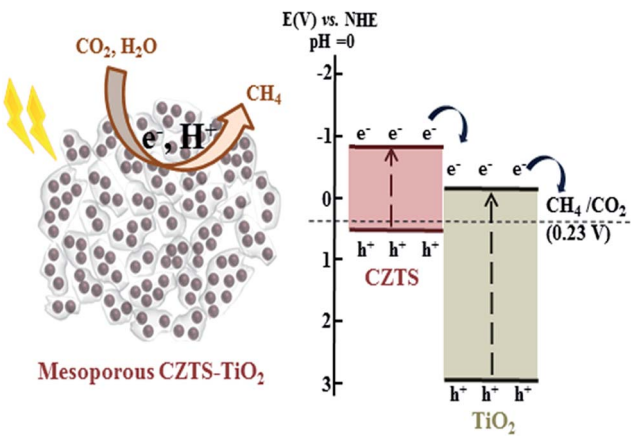

Fig. 8 Schematic illustration for photocatalytic CO_2 conversion into methane by hybrid CZTS–TiO_2 samples with proposed energy level diagram.

adsorbed H_2O. Photoreduction of CO_2 is a multi-electron process, requiring reaction of 8 holes (h^+) with adsorbed H_2O, producing O_2 and H^+ ions and reducing the CO_2 adsorbed on photocatalyst surface *via* reaction of 8 electrons (e^-) and 8 protons (H^+ ions), evolving CH_4 as the dominant product.[40]

Sample stability is investigated by testing sample CT4 under up to 10 h of continuous illumination for CO_2 photoreduction (Fig. S8†). It is observed that the methane production rate after 5 h illumination slightly increases from the 1 h value, whereas a 40% decrease in the methane production rate is observed after 10 h of continuous illumination. We are unsure of the origin of such behavior, but such behavior is not unusual in the realm of photocatalysts.

4. Conclusions

We have successfully synthesized a hybrid mesoporous CZTS–TiO_2 photocatalyst using a simple two-step process. The hybrid CZTS–TiO_2 samples exhibit improved light absorption and mesoporosity mainly induced by CZTS content. The as-prepared samples are characterized by various analytical techniques such as XRD, TEM, UV-vis DRS spectra, BET and XPS. A considerable enhancement in CO_2 conversion into methane under AM1.5G illumination is observed for the mesoporous CZTS–TiO_2 samples, which we attribute to improved light absorption, large surface areas which in turn promote higher interfacial reactions, and intrinsic formation of a p–n junction between the CZTS and TiO_2 regions with formation with suitable bandgap edge positions for improved charge separation. Our material synthesis strategy, and coupling of favorable semiconductors suggests an effective approach for design of high performance noble metal free photocatalyst materials.

Acknowledgements

The authors gratefully acknowledges the support by the DGIST R&D Program of the Ministry of Education, Science and Technology of Korea (16-BD-0404) and by Basic Science research program through the National Research Foundation of Korea funded by the Ministry of Science, ICT & Future Planning (2013R1A1A008678 & 2014K1A3A1A47067086). This research was also supported by the Technology Development Program to Solve Climate Changes of the National Research Foundation (NRF) funded by the Ministry of Science, ICT & Future Planning(2015M1A2A2074670). The authors are thankful to DGIST R&D Program and MIREBraiN Program of the Ministry of Science, ICT & Future Planning (15-01-HRSS01 & 201510023).

References

1 P. Tans, *Trends in atmospheric carbon dioxide*, http://www.esrl.noaa.gov/gmd/ccgg/trends/, accessed, 07, 2015.
2 S. N. Habisreutinger, L. S. Mende and J. Stolarczyk, *Angew. Chem., Int. Ed.*, 2013, **52**, 7372–7408.
3 Q. Liu, Y. Zhou, J. Kou, X. Chen, Z. Tian, J. Gao, S. Yan and Z. Zou, *J. Am. Chem. Soc.*, 2010, **132**, 14385–14387.
4 M. R. Hoffmann, S. T. Martin, W. Choi and D. W. Bahnemann, *Chem. Rev.*, 1995, **95**, 69–96.
5 S. U. Khan, M. Al-Shahry and W. B. Ingler Jr, *Science*, 2002, **297**, 2243–2244.
6 X. Wu, Z. Chen, G. Q. M. Lu and L. Wang, *Adv. Funct. Mater.*, 2011, **21**, 4167–4172.
7 P. Yaron, *Appl. Catal., B*, 2010, **99**, 448–460.
8 S. K. Dutta, S. K. Mehetor and N. Pradhan, *J. Phys. Chem. Lett.*, 2015, **6**, 936–944.
9 N. Roy, Y. Sohn, K. M. Leung and D. Pradhan, *J. Phys. Chem. C*, 2014, **118**, 29499–29506.
10 X. Liu, J. Chen, J. Li and C. Burda, *Chemosphere*, 2005, **61**, 11–18.
11 J. C. Yu, L. Zhang, Z. Zheng and J. Zhao, *Chem. Mater.*, 2003, **15**, 2280–2286.
12 T. Hirai, K. Suzuki and I. Komasawa, *J. Colloid Interface Sci.*, 2001, **244**, 262–265.
13 D. Chatterjee and A. Mahata, *Appl. Catal., B*, 2001, **33**, 119–125.
14 J. Wang, T. Ma, G. Zhang, Z. Zhang, X. Zhang, Y. Jiang, G. Zhao and P. Zhang, *Catal. Commun.*, 2007, **8**, 607–611.
15 S. K. Parayil, A. Razzaq, S. M. Park, C. A. Grimes and S. l. In, *Appl. Catal., A*, 2015, **498**, 205–213.
16 M. Zhu, C. Zhai, L. Qiu, A. S. Paton, Y. Du and M. C. Goh, *ACS Sustainable Chem. Eng.*, 2015, **3**, 3123–3129.
17 Y. Lu, D. Chu, M. Zhu, Y. Du and P. Yang, *Phys. Chem. Chem. Phys.*, 2015, **17**, 17355–17361.
18 S. Song, B. Cheng, N. Wu, A. Meng, S. Cao and J. Yu, *Appl. Catal., B*, 2016, **181**, 71–78.
19 A. Razzaq, C. A. Grimes and S. I. In, *Carbon*, 2016, **98**, 537–544.
20 X. Xin, M. He, W. Han, J. Jung and Z. Lin, *Angew. Chem., Int. Ed.*, 2011, **50**, 11739–11742.
21 L. Shi, C. Pei, Y. Xu and Q. Li, *J. Am. Chem. Soc.*, 2011, **133**, 10328–10331.
22 H. Yang, L. A. Jauregui, G. Zhang, Y. P. Chen and Y. Wu, *Nano Lett.*, 2012, **12**, 540–545.
23 S. C. Riha, B. A. Parkinson and A. L. Prieto, *J. Am. Chem. Soc.*, 2009, **131**, 12054–12055.
24 H. Kim, A. Razzaq, H. J. Heo and S. I. In, *Rapid Communication in Photoscience*, 2013, **2**, 64–66.
25 N. Muhunthan, O. P. Singh, S. Singh and V. N. Singh, *Int. J. Photoenergy*, 2013, **752012**, 1–7.
26 P. A. Sedach, T. J. Gordon, S. Y. Sayed, T. Fürstenhaupt, R. Sui, T. Baumgartner and P. C. P. Berlinguette, *J. Mater. Chem.*, 2010, **20**, 5063–5069.
27 D. R. Coronado, G. R. Gattorno, M. E. E. Pesqueira, C. Cab, R. Coss and G. Oskam, *Nanotechnology*, 2008, **19**, 1–10.
28 P. Kush, S. K. Ujjain, N. C. Mehra, P. Jha, R. K. Sharma and S. Deka, *ChemPhysChem*, 2013, **14**, 2793–2799.
29 J. J. Scragg, T. Ericson, T. Kubart, M. Edoff and C. P. Björkman, *Chem. Mater.*, 2011, **23**, 4625–4633.
30 A. Weber, R. Mainz and H. W. Schock, *J. Appl. Phys.*, 2010, **107**, 013516-1–013516-6.
31 S. P. Lim, A. Pandikumar, N. M. Huang, H. N. Lim, G. Gud and T. L. Ma, *RSC Adv.*, 2014, **4**, 48236–48244.

32 T. Kameyama, T. Osaki, K. Okazaki, T. Shibayama, A. Kudo, S. Kuwabata and T. Torimoto, *J. Mater. Chem.*, 2010, **20**, 5319–5324.
33 X. Yin, C. Tang, M. Chen, S. Adams, H. Wang and H. Gong, *J. Mater. Chem. A*, 2013, **1**, 7927–7932.
34 B. Lu, X. Wang, G. Cai, L. Wen, Y. Song and X. Zhao, *J. Hazard. Mater.*, 2009, **169**, 1112–1118.
35 H. Tang, F. Lévy, H. Berger and P. E. Schmid, *Phys. Rev. B: Condens. Matter Mater. Phys.*, 1995, **52**, 7771–7774.
36 S. Sarkar, K. Bhattacharjee, G. C. Das and K. K. Chattopadhyay, *CrystEngComm*, 2014, **16**, 2634–2644.
37 P. Dai, X. Shen, Z. Lin, Z. Z. Feng, H. Xu and J. Zhan, *Chem. Commun.*, 2010, **46**, 5749–5751.
38 M. Kruk and M. Jaroniec, *Chem. Mater.*, 2001, **13**, 3169–3183.
39 S. P. Dilsaver, M. D. Reichert, B. L. Hallmark, M. J. Thompson and J. Vela, *J. Phys. Chem. C*, 2014, **118**, 21226–21234.
40 S. K. Parayil, A. Razzaq, S. M. Park, H. R. Kim, C. A. Grimes and S. I. In, *Appl. Catal., A*, 2015, **498**, 205–213.